On the Role of Dust-Deposited Lithogenic Particles for Iron Cycling in the Tropical and Subtropical Atlantic

Y. Ye[1] (ID) **and C. Völker[1]** (ID)

[1]Helmholtz Centre for Polar and Marine Research, Alfred Wegener Institute, Bremerhaven, Germany

Abstract Lithogenic material deposited as dust is one of the major sources of trace metals to the ocean, particularly in the tropical and subtropical Atlantic. On the other hand, it can also act as a scavenging surface for iron. Here we studied this double role of lithogenic material in the marine iron cycle by adding a new scheme for describing particle dynamics into a global biogeochemistry and ecosystem model including particle aggregation and disaggregation of two particle size classes and scavenging on both organic and lithogenic particles. Considering the additional scavenging of iron on lithogenic particles, the modeled dissolved iron concentration is reduced significantly in the tropical and subtropical Atlantic, bringing the model much closer to observations. This underlines the necessity to consider the double role of dust particles as iron source and sink in studies on the marine iron cycle in high dust regions and with changing dust fluxes.

1. Introduction

Lithogenic material, carried by the atmosphere and deposited as dust, is a major source of trace metals to the ocean (Duce & Tindale, 1991; Guieu et al., 2014; Jickells et al., 2005). Especially for iron, which is an important micronutrient for phytoplankton (Geider & La Roche, 1994), the input of dust has been hypothesized to be an important driver of marine primary and export production on time scales ranging from subseasonal (Bishop et al., 2002) to glacial-interglacial (Martin, 1990). Other external sources of iron have over the last decade been shown to be important as well and also to outweigh dust deposition regionally (Elrod, 2004; Resing et al., 2015; Tagliabue et al., 2010; Wadley et al., 2014). In the tropical and subtropical Atlantic, which receives at least half of the global deposition flux of dust to the oceans (Mahowald et al., 1999), however, dust is very likely to be the dominant source of iron to the surface ocean, and its influence is clearly reflected in the distribution of dissolved iron (Measures et al., 2008; Sarthou et al., 2007; Ussher et al., 2013). The dominant role of dust as iron source to the Atlantic has also been confirmed by studies of the stable isotopic composition of dissolved and particulate iron (Conway & John, 2014; Revels et al., 2015).

Iron, on the other hand, is very insoluble in seawater (Liu & Millero, 2002) and has a strong tendency to adsorb onto particle surfaces present in seawater, in a process called scavenging. Scavenging occurs predominantly via the formation of colloidal nanoparticles that subsequently aggregate onto larger sinking particles (Honeyman & Santschi, 1989; Rose & Waite, 2007). Dust deposition, besides being a source of iron, also is a source of particles and hence scavenging surface; this explains why the addition of dust can also lead to a decrease of dissolved iron (Wagener et al., 2010).

In most circumstances in the open ocean, suspended particulate matter is dominated by biogenic particles, while lithogenic particles are only a minor fraction. This, however, is not necessarily true in the high dust regions downwind of the Sahara, where a substantial fraction of the particles can be of lithogenic origin (Lam et al., 2015; Ohnemus & Lam, 2015). It is primarily in these regions that dust may play a double role both as source and sink of dissolved iron (Ye et al., 2011). Quantifying this double role, however, is made difficult by the fact that the concentration of dust particles in the ocean is shaped by intensive aggregation-disaggregation processes (Ohnemus & Lam, 2015; Ye et al., 2011), which complicate the estimation of lithogenic particle concentration directly from dust deposition.

In this study, we attempt to quantify the effect of dust both as a source and a sink for iron in the Atlantic Ocean by means of a global biogeochemical model. Different descriptions of the iron sink by scavenging have been applied in global iron models: some still use a first-order uniform scavenging rate, and some make it

dependent on concentration of biogenic particles (Tagliabue et al., 2015). There are also models (e.g., Aumont et al., 2015), which include a scavenging term on lithogenic particles but make drastic assumptions on the dynamics of lithogenic particles, namely, a uniform constant sinking speed and no aggregation. Our model takes into account a complex cycle of lithogenic particles including aggregation and disaggregation, as well as adsorption of iron onto both biogenic and lithogenic particles. We take advantage of the fact that with the international GEOTRACES effort, there is a growing database of both dissolved and particulate trace element concentration measurements that we use to test our model predictions. Specifically, we aim to (1) investigate the influence of aggregation and disaggregation the distribution of lithogenic material, (2) check whether the inferences based on our model on this role are compatible with earlier hypotheses based on observations (Barrett et al., 2012) and one-dimensional modeling (Barkmann et al., 2010; Ohnemus & Lam, 2015), (3) quantify the role of the lithogenic particle pool as additional scavengers for iron in the Atlantic, and (4) check whether inclusion of a simple scheme for lithogenic particles and their role as scavengers decreases model-data mismatch for dissolved iron in high dust flux regions.

To this end, we have added a new scheme for describing lithogenic particle dynamics (section 2) into our global biogeochemistry and ecosystem model REcoM (Hauck et al., 2013). The aggregation model is fairly simplistic compared to those described, for example, in Jackson and Burd (1998) and Burd (2013), but allows for horizontal transport of particles, in contrast to the one-dimensional models of Ohnemus and Lam (2015) and Barkmann et al. (2010). In section 3.1, we compare the predictions made with this model with a number of recent studies on particulate trace metals in the Atlantic; in section 3.2, we investigate how well the aggregation rates that we obtain from our model compare to published rate estimates based on thorium measurements; we then study modeled distributions of dissolved iron both with and without inclusion of the scavenging role of lithogenic material (section 3.3); and finally, we discuss the model results and their shortcomings (section 4) and draw conclusions on the role of lithogenic particles in the cycling of iron in the Atlantic (section 5).

2. Model Description

2.1. The Physical and Biogeochemical Model

The ocean circulation model that we use to calculate the transport of all tracers through advection and diffusion is a nearly global setup of the Massachusetts Institute of Technology circulation model (Marshall et al., 1997), spanning the latitude range from 80°N to 80°S at a zonal resolution of 2° and a meridional resolution between 0.39° and 2°. In the vertical it has 30 layers, increasing in thickness from 10 m at the surface to 500 m below a depth of 3,700 m. The model includes a dynamic sea ice model (Losch et al., 2010), and we use the Gent-McWilliams parameterization for turbulent tracer and momentum fluxes (Gent & McWilliams, 1990) and a bottom boundary layer scheme (Campin & Goosse, 1999) for improving the representation of overflows.

To this physical model setup we have coupled a marine ecosystem and biogeochemical model, REcoM2, described in detail in Hauck et al. (2013) and Hauck and Völker (2015). REcoM2 describes two phytoplankton classes, diatoms and nondiatoms; a generic zooplankton; and one class of organic sinking particles which is assumed to be aggregates with a sinking speed that increases with depth (Kriest & Oschlies, 2008). The model for phytoplankton growth is based on a quota approach (Geider et al., 1998) and allows for variable cellular C:N:Chl:(Si,Fe) stoichiometry (Schartau et al., 2007). The iron cycle in the model is driven by dust and sedimentary inputs of iron, biological uptake and remineralization, and scavenging onto particles.

2.2. Lithogenic Particles in the Model

We have two lithogenic particle classes: fine dust P_s and the lithogenic part in aggregates P_l (Figure 1). Concentrations in the model are in mg m^{-3}. We assume that the dust that is deposited is mostly fine, <1 μm diameter, so it sinks only slowly on its own, with a constant sinking speed w_s of 0.2 m d^{-1}.

We consider two types of particle aggregation: the aggregation between dust particles with a second-order mass specific aggregation rate k_{c_1} and that between dust and biogenic aggregates with k_{c_2} which is kept in a fixed ratio to k_{c_1}. We chose a ratio of 3:1 based on the ratio of the rate constants calculated using a size spectrum model for the curvilinear coagulation kernels by Burd (2013) and the model parameters in Ye et al. (2011), which simulated the effect of dust addition on iron cycling in a mesocosm experiment.

The aggregates in our model sink as a whole, that is, we assume the same sinking speed w_l for the lithogenic part of aggregates as for detritus which increases linearly with depth, with 20 m d^{-1} at the surface and 50 m d^{-1}
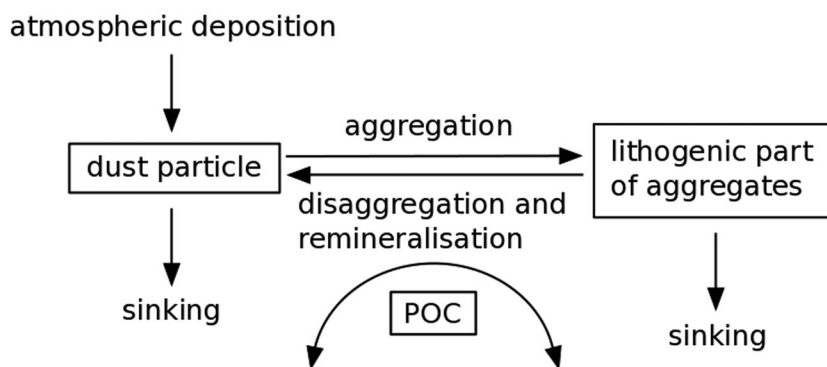
Figure 1. Lithogenic particles and their sources and sinks in the model.

at 1,000 m. When detritus is remineralized with a (temperature-dependent) rate k_r, part of the lithogenic material is released again in the form of fine dust particles, in such a way that the lithogenic fraction in the aggregates is conserved, for example, at the same rate as the remineralization. Furthermore, we have an additional term for disaggregation, with a disaggregation rate k_{diss}.

Taken together, the model equations for the two components are thus (symbolizing advection and diffusion terms for simplicity by F_s and F_l)

$$\frac{\partial}{\partial t}P_s = F_d - k_{c_1} \cdot P_s{}^2 - k_{c_2} \cdot (P_l + r_{C:m}D) \cdot P_s + \left(k_r + k_{diss}\right)P_l - \frac{\partial}{\partial z}\left(w_s P_s\right) + F_s \qquad (1)$$

$$\frac{\partial}{\partial t}P_l = k_{c_1} \cdot P_s{}^2 + k_{c_2} \cdot (P_l + r_{C:m}D) \cdot P_s - \left(k_r + k_{diss}\right)P_l - \frac{\partial}{\partial z}\left(w_l P_l\right) + F_l. \qquad (2)$$

The source of small particles from dust deposition F_d is zero everywhere except in the first layer, where it is the dust deposition flux (in mg m^{-2} d^{-1}) divided by the first model layer depth. Organic detritus D (in mmol C m^{-3}) is converted into mass units with the conversion factor $r_{C:m} = 24$ g biomass mol C^{-1} (assuming that carbon is half the biomass).

Based on an extensive sensitivity study with respect to aggregation and disaggregation rates (sections A1 and A2), we use a value of $2.6 \cdot 10^{-2}$ (mg/m^3)$^{-1}$ d^{-1} for the aggregation between small particles (k_{c_1}) and a disaggregation rate of 2.5 d^{-1} (k_{diss}). In section 3.2, we calculate the first-order aggregation rates in the model $r_{aggr} = k_{c_1} \cdot P_s + k_{c_2} \cdot (P_l + r_{C:m}D)$ and compare them with estimates made using thorium data.

Organic complexation of dissolved iron is considered in the model, using a constant ligand concentration of 1 μmol m^{-3}. Iron that is not bound to organic ligand undergoes adsorption onto surfaces of both detritus (biogenic particles) and lithogenic particles including dust particles and the lithogenic part of aggregates. Different scavenging rate constants are assumed for these two kinds of particles: $1.56 \cdot 10^{-2}$ (mmol C/m^3)$^{-1}$ d^{-1} for scavenging onto biogenic particles, resulting from former sensitivity studies (Hauck et al., 2013) and $7.5 \cdot 10^{-4}$ (mg/m^3)$^{-1}$ d^{-1} for scavenging onto lithogenic particles, adapted from our 1-D model for a dust addition experiment (Ye et al., 2011).

2.3. Model Experiments and Setup

Model experiments were started from a state of rest and a temperature and salinity distribution interpolated from the World Ocean Atlas 2009 (Antonov et al., 2010; Locarnini et al., 2010). Dissolved inorganic nitrogen and silicate were also taken from the World Ocean Atlas, dissolved inorganic carbon, and alkalinity from Global Ocean Data Analysis Project (Key et al., 2004). Model output from Aumont et al. (2015) was used as initial dissolved iron. All other variables of the ecosystem model were initialized with small constant values.

After initialization, model runs were integrated for 100 years, enough to get the iron cycle and the particle concentrations into a cyclostationary state. Model output from the last 10 years was taken for analysis. Model runs were driven by the daily (except for monthly precipitation) normal year atmospheric forcing fields from the coordinated ocean research experiments (CORE) (Large & Yeager, 2008); a climatology of monthly dust deposition fields was taken from Mahowald et al. (2005). We assume that dust contains 3.5% of iron and an immediate dissolution of iron from deposited dust particles with a solubility of 2%.
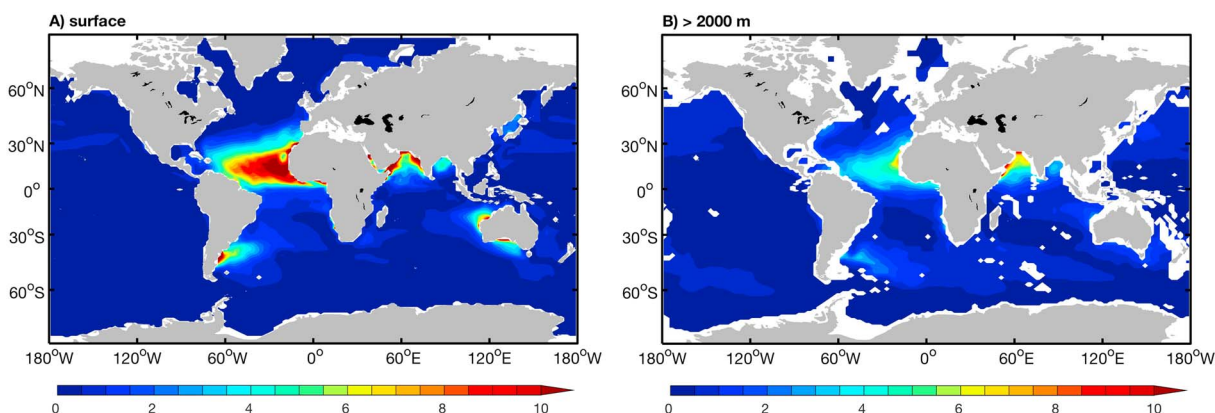
Figure 2. Lithogenic suspended particulate matter (annual average in mg m^{-3}) at the (a) surface and vertically averaged below (b) 2,000 m depth.

Two model runs are presented in this paper: one with ("+Lith") and one without ("−Lith") the scavenging effect of lithogenic particles. In addition, 40 sensitivity runs have been performed with respect to processes affecting the particle cycle. Their parameter values and results of some of them can be found in sections A1 and A2.

3. Results

3.1. Particles and Particulate Iron Concentrations

The concentration of lithogenic suspended particles, that is, the sum of lithogenic material in dust and in larger aggregates ($P_s + P_l$), at the ocean surface shows elevated values only in regions directly under the dust plumes downwind of the major deserts, especially the Sahara (Figure 2a). Somewhat elevated values are also found in the Arabian Sea, near Patagonia and Australia, but do not extend as far into the open ocean as in the Atlantic. In the rest of the ocean, lithogenic particle concentrations are generally negligible compared to biogenic particles. This pattern indicates a relatively short residence time of the slow-sinking dust particles at the surface compared to the time scales of horizontal advection and a rapid removal through aggregation. At depth, the fine fraction dominates the lithogenic particles, leading to a longer residence time of the lithogenic iron. The lateral advection of this fine dust fraction results in a slightly more homogenous distribution than at the surface (Figure 2b). The highest concentrations, nevertheless, are found in the vicinity of the main dust deposition regions.

The modeled distributions of lithogenic particles can be compared to concentrations of particulate iron (pFe) that were measured on two occupations of the CLIVAR A16N cruise (Figure 3d) in the Atlantic in summer 2003 and 2013 (Barrett et al., 2012, 2015) and along a Polarstern cruise in winter 2005 (Pohl et al., 2011). All three cruises found elevated values of pFe under the Saharan dust plume, with typical surface values under the plume ranging between 2 and 8 μmol m^{-3} (Pohl et al., 2011), 2.4 to 3.4 μmol m^{-3} (Barrett et al., 2012), and 2 to 7 μmol m^{-3} (Barrett et al., 2015). The modeled maximum surface pFe concentration is in the same range but located some degrees to the north of the observations (Figure 3a), probably caused by the difference between the climatology of dust deposition used in the model and the individual dust events during the cruises.

In the vertical, Barrett et al. (2012, 2015) both generally find a subsurface minimum at depths between 100 and 200 m, where concentrations are lower by 1–2 μmol m^{-3} under the dust plume than at the surface (Figure 3b). They ascribe this to the rapid export of particles in aggregates. Below this minimum, there is a maximum between the equator and 20°N, with mean values calculated between 200 m and 1,000 m depth of 3.4 μmol m^{-3} in 2003 and 4.3 μmol m^{-3} in 2013. Barkmann et al. (2010) also showed similar profiles of modeled and observed dust concentrations in the Arabian Sea.

We find a very similar pattern in the model (Figure 3a) with highest concentrations of 4–6.5 μmol m^{-3} at the surface under the Saharan dust plume (5–25°N), followed by a rapid decrease to a subsurface minimum between 100 and 200 m. The concentrations are lower by 1–2.5 μmol m^{-3} (~20–40%). This is mainly caused by strong particle aggregation that is reflected in the distribution of coarse lithogenic iron (Figure 3c). The coarse fraction of pFe reaches 35% at the subsurface minimum of total pFe. The subsurface minimum of total pFe is less clear around 20°N, since particle aggregation between dust and large particles is much weaker in the subtropical gyre due to the low concentration of biogenic particles. Below the subsurface minimum,
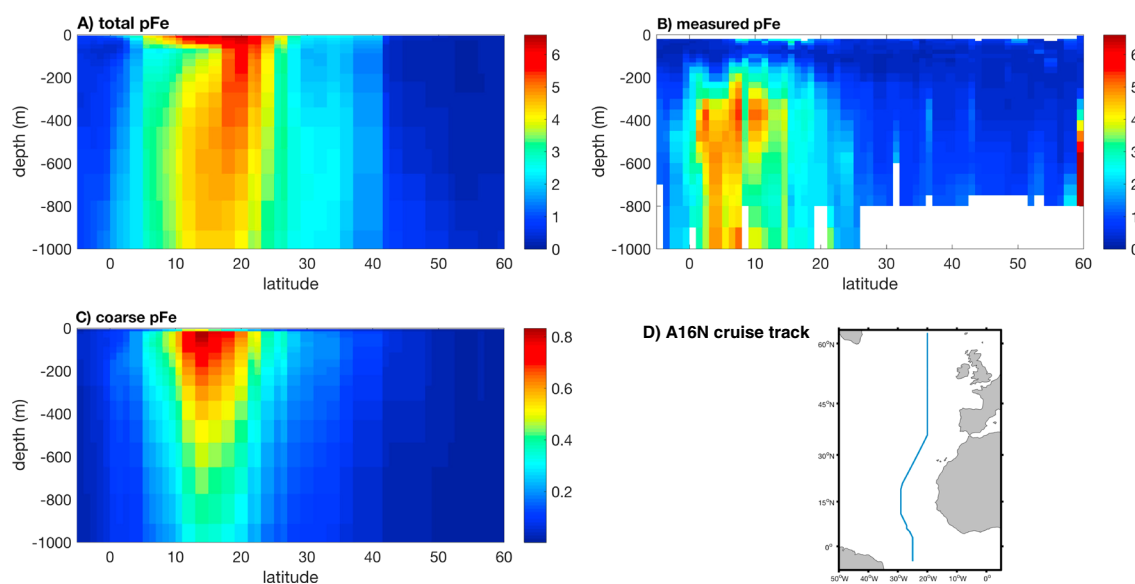
Figure 3. Particulate iron (μmol Fe m^{-3}) along the CLIVAR A16N section in the tropical and North Atlantic: (a) modeled iron contained in all lithogenic particles, (b) measured particulate iron provided by Pamela Barrett, (c) modeled iron contained in the lithogenic part of aggregates only, and (d) the cruise track of A16N. Color scales of the modeled data are different.

remineralization and disaggregation slow down the export of particles and lead to an increase of pFe up to 4.5 μmol m^{-3}. Here we ignore the iron scavenged on the particle surface and contained in living organisms because of their minimal contribution to the total particulate iron in the water column compared to iron in the lithogenic particles. In regions without significant input of lithogenic particles, the role of scavenged and biological particulate iron must be taken into account.

One discrepancy between the observed and modeled pattern of pFe is that the observed pFe concentration at the surface under dust plume is lower than that at the deep maximum, whereas the highest concentration is found at the surface in the model, independent of the aggregation rates used in the model (section A2). One possible reason could be that we use monthly averaged dust deposition fields in the model. Dust deposition brings lithogenic particles to the ocean surface intermittently. Particle aggregation is described in the model with quadratic functions and thus acts nonlinearly on the distribution of deposited lithogenic particles. By averaging the deposition flux monthly, we miss the intermittent high input of dust particles by individual dust events and thus may have weakened the subsequent transport of lithogenic particles into the ocean interior by particle aggregation. This could also explain the lower fraction of coarse lithogenic particles in our model than in the measurements by Ohnemus and Lam (2015) (section A3). The second reason could be that the dust deposition fields by Mahowald et al. (2005) may overestimate the deposition in the eastern tropical North Atlantic Ocean (Anderson et al., 2016). Another reason could be the simplicity of the particle dynamics in the model, for example, the uniform sinking velocity of all kinds of aggregates at the same depth, independent of their composition and size. If this is appropriate for aggregates mainly consist of lithogenic particles remains to be examined if more data on the vertical distribution of lithogenic particles become available.

3.2. Aggregation and Disaggregation Rate

Rate constants of particle aggregation and disaggregation have been estimated in a few studies from measurements of particle-reactive metals, in particular, thorium. Globally, the estimated first-order aggregation rates range from 0.02 to 640 y^{-1} and disaggregation rates from 16 to 5,000 y^{-1} (Lam et al., 2015). For a direct comparison with these estimates, we calculated a quasi first-order total aggregation rate r_{aggr} for small particles from the modeled aggregation rates that depends on the concentration of small and large particles:

$$r_{\text{aggr}} = k_{c1} \cdot P_s + k_{c2} \cdot \left(P_l + r_{C:m}D \right) . \tag{3}$$

Our model represents a similar but wider range of aggregation rates, and the disaggregation rate is within the range of the estimates (Table 1). One should, however, be cautious when comparing model rates and

Table 1
Comparison of Model Rate Constants (y^{-1}) With Some Published Estimates

r_{aggr}	r_{disag}	Region	Study
0.01 – 1800	900	Global	Our model
2.5 – 12.3	148 – 788	Northwest Pacific	Nozaki et al. (1987)
3.72 – 642.4	150 – 3,760	Northeast Pacific	Clegg and Whitfield (1991)
0.8	400	Northeast Pacific	Murnane (1994)
0.02 – 49	16 – 4,996	Eastern equatorial Pacific	Clegg et al. (1991)
1.1 – 33.2	126 – 407	North Atlantic	Cochran et al. (1993)
8 – 18	580 – 2,690	North Atlantic	Murnane et al. (1994)
2 – 76	156 – 524	North Atlantic	Murnane et al. (1996)

Note. r_{aggr}: aggregation rate and r_{disag}: disaggregation rate.

estimates because (1) all the thorium-based models used to estimate these rate constants assume first-order kinetics for aggregation between small particles, whereas we assume second-order kinetics for aggregation between small particles and for aggregation between small particles and aggregates; (2) different assumptions and methods have been used to solve for the rate constants, for example, direct or least squares methods, resulting in relatively high uncertainties and limited comparability within the estimates; (3) the compilation by Lam et al. (2015) mainly covers the North Atlantic, the equatorial, and North Pacific. More data sets would be needed for a comparison of the geographic pattern. Therefore, we roughly compare the range of the model values with the estimates and do not further constrain the model with these rate constants.

The ratio of disaggregation to aggregation rate has been used to illustrate the dominant process in particle dynamics, for example, lower ratios could indicate formation of large particles and higher vertical particle flux (Lam et al., 2015). At the surface, the ratio of disaggregation to aggregation rates in the model basically follows the inverse pattern of the global primary production (Figure 4a): the highest ratios are found in the subtropical gyres and lower values in regions with high biological productivity. This is not surprising because higher abundance of biological particles accelerates the formation of aggregates, leading to higher vertical flux through the water column. The ratio in the North Atlantic Gyre is significantly lower than that in other gyres, because the atmospheric input and the advective transport of dust particles contribute to the vertical particle flux via aggregation. And the higher productivity there also results in a higher flux of particulate organic matter.

In vertical, the ratio of disaggregation to aggregation rate increases with depth (Figure 4), caused by the dropoff of the productivity-driven aggregation away from the surface. This vertical variability is consistent with the majority of the estimates based on thorium data (Lam et al., 2015) and the modeling study by Ohnemus and Lam (2015).
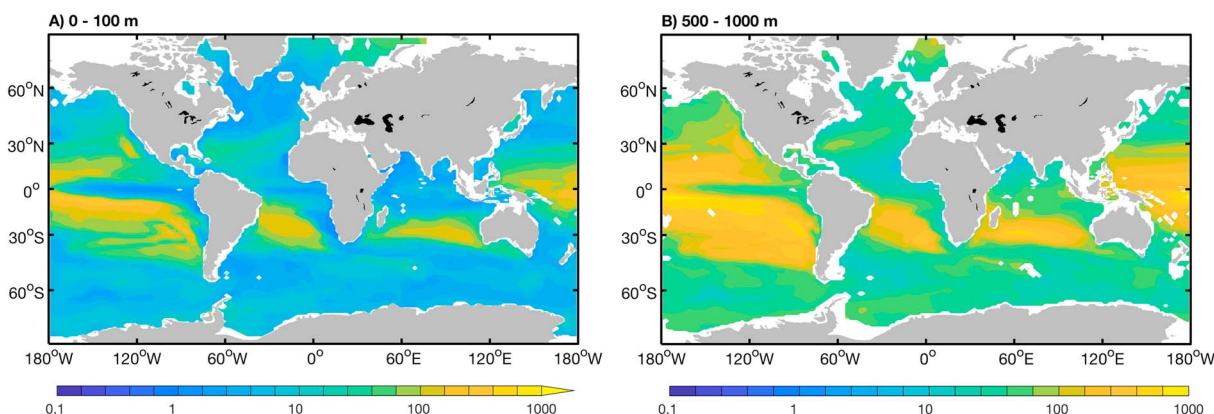

Figure 4. Ratio of disaggregation to aggregation rate in the model averaged in the upper (a) 100 m and between (b) 500 and 1,000 m.
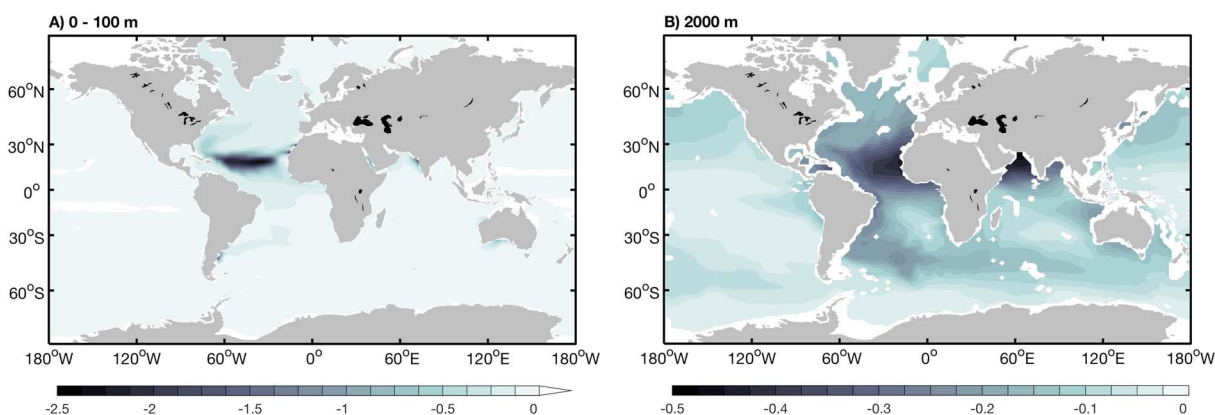
Figure 5. Change of dissolved iron concentration (μmol Fe m^{-3}) in +Lith relative to −Lith at the (a) surface and (b) 2,000 m depth. Color scales of the two plots are different.

3.3. Effect of Lithogenic Particles on Dissolved Iron

We illustrate the effect of lithogenic particles on the distribution of dissolved iron by showing the difference in dissolved iron between a run including (+Lith) and a run excluding (−Lith) the role of lithogenic material as iron scavengers (Figure 5). Surface concentrations of dissolved iron in +Lith are lower mainly in the high dust deposition regions. The largest decrease up to 2.5 μmol m^{-3} in +Lith relative to −Lith is found in the North Atlantic basin center around ~15°. There is no significant effect close to the African coast where the highest dust deposition takes place. The high biological productivity near the coastal upwelling leads to both a high biological iron uptake and a high abundance of biogenic particles that can act as iron scavengers (section 4.3 and Figure 8). The excess iron there is already low and the additional scavenging onto lithogenic particles is, therefore, weaker than in the center of the basin. At depth, the two runs also show a significant difference which is much more widespread, ranging from ~0.5 μmol m^{-3} under the dust plume in the Atlantic and Arabian Sea to ~0.2 μmol m^{-3} along the spreading path of the North Atlantic Deep Water to relatively small changes in the deep Pacific.

4. Discussion

4.1. Modeled and Observed Dissolved Iron

We compare the model results with measured surface concentrations of dissolved iron in the Atlantic Ocean (Figure 6). In the absence of scavenging by lithogenic particles, iron is scavenged only by biogenic particles. One would therefore expect high concentration of dissolved iron in the tropical and subtropical North Atlantic where much iron is deposited by dust events, but scavenging is low due to relatively low biological productivity, which is indeed observed in −Lith (Figure 6a). Iron concentrations in this region are also elevated in the observations but far from the magnitude found in −Lith.

In +Lith (Figure 6b), iron concentrations in the tropical and subtropical Atlantic are much closer to the observations. Dust deposition leads to an increase of dissolved iron up to ~1 μmol m^{-3} higher than the rest of the Atlantic Ocean. At the same time, the deposited fine lithogenic particles provide a large surface for iron adsorption and particle aggregation, increasing net scavenging loss and limiting the accumulation of dissolved Fe found in −Lith. Therefore, the enhancement of dissolved iron here is not as intensive as in −Lith. The observed iron concentrations along the northwestern African coast are not as high as in the open ocean downwind the Saharan desert. This pattern is also reflected in our model and caused by high biological uptake and abundance of both lithogenic and biogenic particles in the coastal region. Directly under the Saharan dust plume, however, modeled concentrations are still a bit higher than observed. A possible reason could be that most measurements took place in summer when the surface iron is fairly exhausted due to phytoplankton growth, whereas we compare it to the annual average of dissolved iron. Another reason could be that the iron input due to wet deposition predominantly consists of colloidal iron (Ussher et al., 2013). Without considering the colloidal pumping (Honeyman & Santschi, 1989), our model might miss an important loss process of dissolved iron, particularly in regions with high wet deposition fluxes or riverine input. Furthermore, a uniform solubility of 2% is applied in the model for calculating the iron input from dust deposition. Using different solubilities of iron for desert-derived and anthropogenically influenced dust and
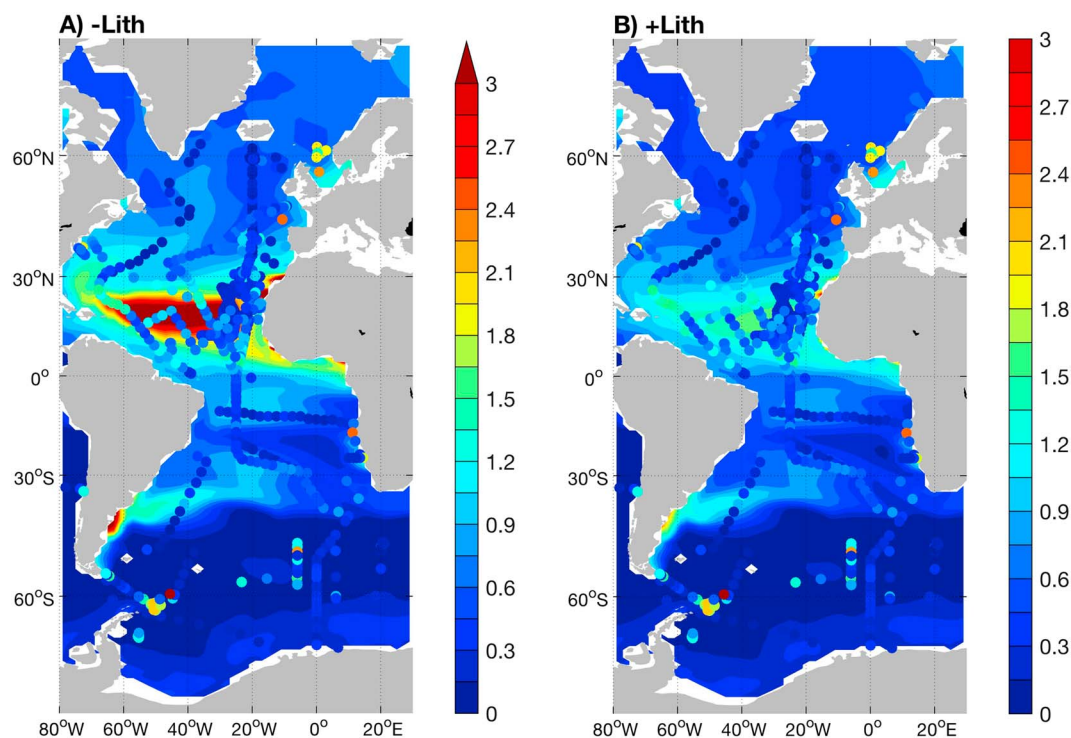
Figure 6. Dissolved iron concentration (μmol Fe m^{-3}) in the upper 50 m in the (a) −Lith and (b) +Lith run. Colored dots indicate measured values from an update of the data compilation by Tagliabue et al. (2012).

considering different degrees of atmospheric processing (Baker & Croot, 2010; Bonnet & Guieu, 2004) might bring the model closer to observations.

4.2. Residence Time of Dissolved Iron

The bioavailability of iron to phytoplankton growth depends not only on the sources of iron but also its residence time in the mixed layer. In some field studies in the Atlantic Ocean, the residence time of dissolved iron has been calculated from the atmospheric input and iron inventories in surface waters: Jickells (1999) reported residence times between 214 and 291 days in the upper 100 m in the Sargasso Sea; longer residence times in the near surface waters were found by Croot et al. (2004), increasing from 280 days to 10.5 years from east to west along a transect at 10°N in the equatorial Atlantic; for the tropical and subtropical Atlantic, residence times on the order of months were estimated by Bergquist and Boyle (2006), with some months for the North Atlantic and up to over a year for the South Atlantic; and Ussher et al. (2013) reported values from 0.4 to 13 years, using data from Atlantic Meridional Transect cruises, and revealed a similar disparity between the North and South Atlantic Ocean. The difference between these estimates is partly caused by their different assumptions on Fe solubility from dust particles, which ranged from 1 to 10%. Other factors like the seasonality of dissolved iron concentrations and atmospheric input may also play a role.

We calculate the mixed layer residence time of dissolved iron τ_{res} based on the inventory of dissolved iron Fe_{mld} and its total sinks in the maximum winter mixed layer, which consists of the adsorptive removal by small lithogenic particles and large aggregates S_{scav} and the removal by phytoplankton uptake S_{upt}:

$$\tau_{res} = \frac{Fe_{mld}}{S_{scav} + S_{upt}}. \tag{4}$$

The modeled mixed layer residence time for the Atlantic Ocean ranges from shorter than 1 day to over 10 years (Figure 7a), comparable to the estimates in field studies. The pattern of residence time is similar to that of the ratio of disaggregation to aggregation rate at the surface (Figure 4a): longer residence times are associated with lower vertical flux of particles. One exception is at the high latitudes. Relatively long residence times from 1 year to over 10 years are found to the north of ~45°N and to the south of ~70°S in the Atlantic sector of the Southern Ocean, which results from deep or complete winter mixing. The increasing trend from east
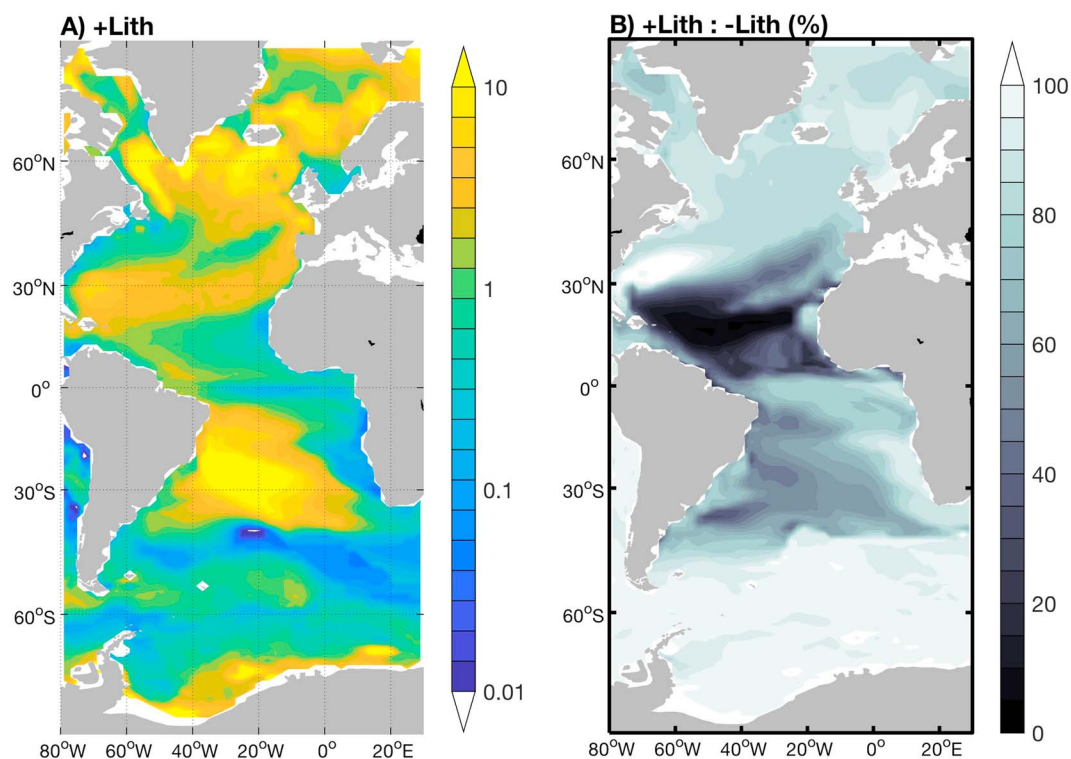
Figure 7. Annual averaged residence time of dissolved iron in the mixed layer: (a) τ_{res} in +Lith (years in a logarithmic scale) and (b) the ratio of τ_{res}^{+Lith} to τ_{res}^{-Lith} (%).

to west along 10°N, found by Croot et al. (2004), is well reproduced in the model. In the South Atlantic Gyre, the highest value exceeds 30 years, whereas in the North Atlantic Gyre it ranges between 3 and 6 years. This is comparable to the north-south difference of 1 order of magnitude demonstrated by Bergquist and Boyle (2006) and Ussher et al. (2013). They ascribe this to high atmospheric input of iron (associated with particles and colloids), high annual productivity, and high particulate organic carbon flux in the North Atlantic.

Comparing to −Lith, the residence time in +Lith is strongly reduced in the tropical and subtropical ocean, particularly in the North Atlantic (Figure 7b). The relative pattern between the north and south gyres is also found in −Lith (not shown here), in other words, the north-south difference is rather determined by the stronger biological uptake and scavenging onto biogenic particles relative to the mixed-layer dissolved iron than by the higher scavenging onto lithogenic particles in the North Atlantic. Just around 30°N in the western part of the subtropical North Atlantic, the residence time in +Lith is slightly longer than that in −Lith. In this region, the concentration of dissolved iron is lower in +Lith (Figure 6), leading to a reduction in biological uptake and abundance of biogenic particles. This in turn lowers the scavenging removal by biogenic particles. Since the additional scavenging onto lithogenic particles does not affect this region considerably (Figure 2), the residence time increases due to the decrease of the biogenic sinks.

The scavenging loss of iron does depend not only on the abundance of sinking particle but also on the amount of iron that is not bound by organic ligands. The model assumption on ligand is therefore crucial for determining the scavenging rate constant. In another model run including a prognostic description of the ligand cycle following Völker and Tagliabue (2015) (not shown), the scavenging rate constant for lithogenic particles needs to be increased strongly to keep the modeled iron concentration within the range of the observations. This dependence of the scavenging loss on ligand variability should be taken into account when comparing residence times of iron in different iron models.

4.3. The Double Role of Dust as Iron Source and Scavenger
Dust deposition has been widely considered as one of the most important external iron sources for the ocean, although the importance of other iron sources like sediments and hydrothermal vents has been recognized during the last decade (e.g., Elrod, 2004; Resing et al., 2015; Tagliabue et al., 2010). To quantify the contribution
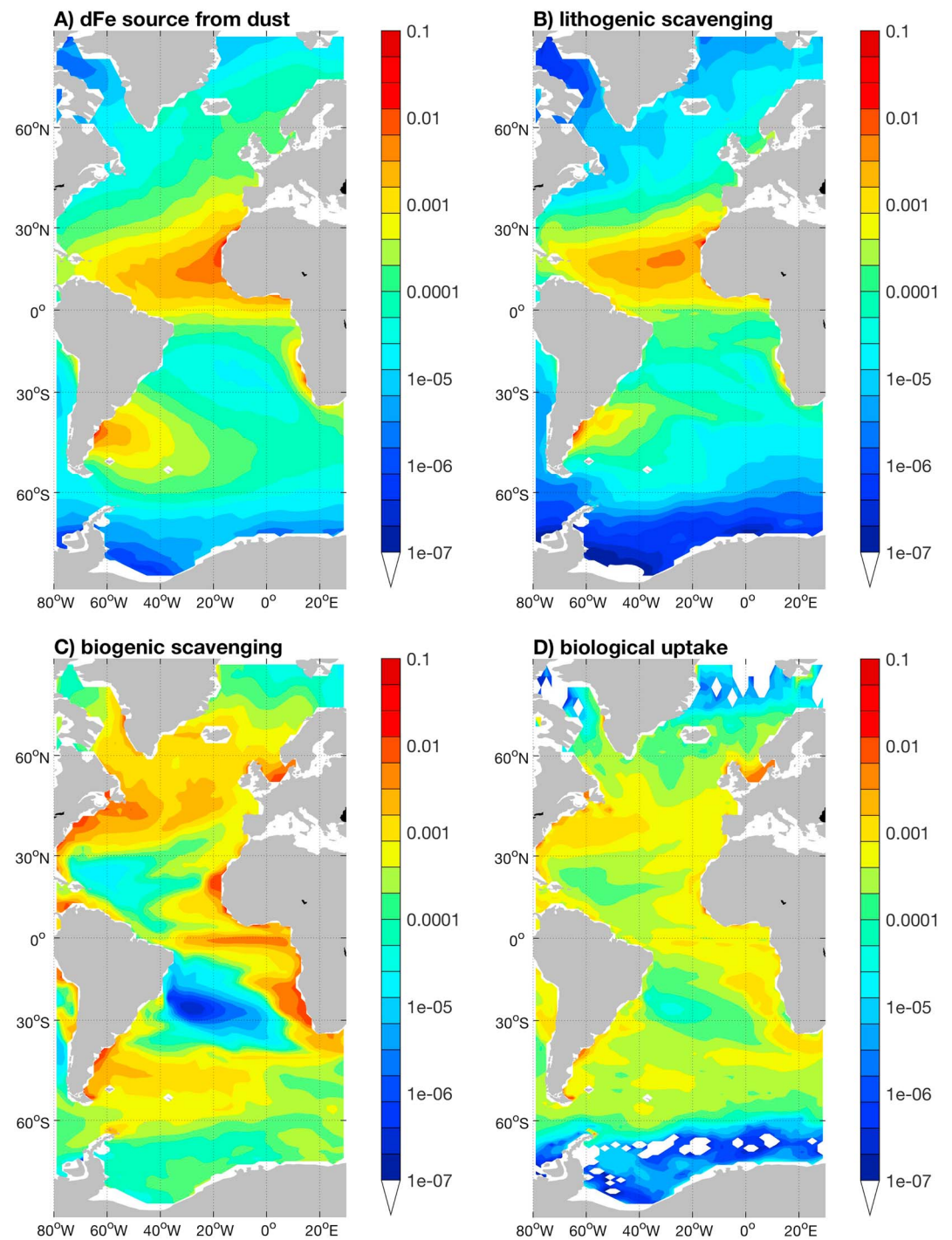
Figure 8. Annual averaged source and sinks of dissolved iron (μmol Fe m^{-3} d^{-1}) in the upper 100 m: (a) iron input by dust deposition, (b) iron loss by scavenging onto lithogenic particles, (c) iron loss by scavenging onto biogenic particles, and (d) iron loss by phytoplankton uptake.

of dust deposition to the global iron budget, it is crucial to take into account the role of the deposited particles in scavenging of dissolved iron, in addition to the total deposition flux and solubility of iron from dust particles. We pointed out in Ye et al. (2011) that dust deposition could even act as a net sink of dissolved iron in regions with high iron concentrations if the scavenging removal exceeds the iron input by dust deposition. In this study, this double role of dust particles has been studied in a 3-D global biogeochemical model, and here we show a quantitative comparison of iron input from dust and the main sinks of iron in the model (Figure 8).

In general, iron input by dust is higher than iron loss by lithogenic scavenging in most parts of the Atlantic (Figures 8a and 8b). But it is worthy to note that dust particles remove iron at a rate in a comparable order of magnitude to that of the iron input by dust. In some regions in the western part of the subtropical North Atlantic, dust deposition could even act as a net sink of dissolved iron. It should, however, be taken into account that we could overestimate the scavenging loss at the surface by assuming an immediate iron dissolution from dust. Biogenic scavenging in most parts of the Atlantic is higher than lithogenic scavenging (Figures 8b and 8c), except in the gyres where the biological activity is low. Due to high input of lithogenic particles by Saharan dust events, lithogenic scavenging in the tropical and subtropical North Atlantic exceeds both biogenic scavenging and phytoplankton uptake and becomes the largest iron sink. In total, dissolved iron is rather removed by physical (scavenging onto all the sinking particles) than biological processes (phytoplankton uptake) (Figure 8d). Only about 1/5 of iron consumed by phytoplankton sinks out of the upper 100 m which results in a even smaller net biological removal.

4.4. Impact on Marine Productivity

Including the lithogenic scavenging in the model mainly changes the surface concentration of dissolved iron in the high deposition regions where biological productivity is limited rather by other nutrients than iron. A decrease of ~3% is still found in the global net primary production and export production, particularly in the high-nutrient low-chlorophyll regions, for example, the equatorial Pacific and Southern Ocean. This demonstrates that lithogenic scavenging has a global effect on marine productivity, even if the amplitude of the total change is small.

The double role of dust as iron source and scavenger is particularly important for assessing the impact of changing dust flux on the marine iron cycle and productivity, for example, during the glacial periods. Ice cores indicate that dust deposition during glacial periods increased by a factor up to 25 comparing to interglacial periods (Lambert et al., 2008; Petit et al., 1999). The enhanced atmospheric iron input has been proposed to cause an increase in marine productivity and export production, contributing to the reduction in the glacial atmospheric CO_2 (Martin, 1990). However, to what extent this higher dust supply could explain the difference in atmospheric CO_2 depends rather on the increase in bioavailable iron than that in the total iron source. Using models considering varying dust fluxes and the biogeochemical cycle of iron but ignoring the concurrent input of lithogenic particles and aggregate formation, one might overestimate the iron supply for marine biota during glacial periods. If this has a significant effect on marine CO_2 uptake remains to be investigated in future modeling studies.

5. Conclusions

In this study, we quantify the double role of dust particles both as a source and a sink of iron in the Atlantic Ocean, by including aggregation of two size classes of particles and disaggregation and differentiated scavenging rates of iron on bogenic and lithogenic particles in a global biogeochemical model. This enables a better description of the spatial variability of the scavenging loss of iron.

Sinking particles in the model are dominated by lithogenic material in regions under dust plumes, for example, the tropical and subtropical Atlantic Ocean, whereas they mainly consist of organic material in the rest of the world ocean. By considering scavenging onto lithogenic particles, modeled dissolved iron concentrations and residence times are significantly reduced in the tropical and subtropical Atlantic Ocean, bringing the model much closer to the observations. In the comparison of the iron source from dust with the different sinks, we show that dust deposition acts as a net iron source in most regions of the Atlantic Ocean; under dust plumes, the iron supply by dust and removal by scavenging onto dust particles are of a comparable order of magnitude, and the biogenic and lithogenic scavenging together is the dominant removal process of dissolved iron compared to biological uptake. These model results underline the necessity to consider the double role of dust particles as iron source and sink in global biogeochemical models of iron. With the growing GEOTRACES database of paired iron and thorium measurements, particularly in the particulate phase, we could better prove our assumptions on aggregation and disaggregation rate constants and further quantify the role of lithogenic particles in the marine iron cycle.

This study focuses on the double role of dust particles in the tropical and subtropical North Atlantic. Other sources of iron (and lithogenic particles) could also be important, for example, nepheloid layers (Lam et al., 2015) and hydrothermal vents (Tagliabue et al., 2010). A significant fraction of iron delivered by these sources (including dust deposition) is in the colloidal size (Bergquist & Boyle, 2006; Lam et al., 2015; Ussher et al., 2013;

Table A1
Parameter Values Changed in Sensitivity Runs (A)

Run	k_{c2}	k_{c1}	k_{diss}	w_s	Name
01	-	-	-	0.2	
02	0.0	-	-	0.2	
03	3.9E−5	-	-	0.2	
04	3.9E−3	-	-	0.2	
05	3.9E−4	–	-	1.0	
06	3.9E−4	-	-	5.0	
07	7.8E−3	-	-	0.2	
08	1.9E−2	-	-	0.2	
09	7.8E−3	-	-	1.0	
10	1.9E−2	-	-	1.0	
11	3.9E−2	-	-	0.2	
12	7.8E−2	-	-	0.2	
13	3.9E−2	-	-	1.0	
14	7.8E−2	-	-	1.0	
15	7.8E−2	-	-	0.2	
16	1.6E−1	-	-	0.2	1 × aggr

Note. k_{c2}: aggregation rate between dust and large particles $((mg/m^3)^{-1}$ $d^{-1})$; k_{c1}: aggregation rate of dust particles $((mg/m^3)^{-1}$ $d^{-1})$; k_{diss}: disaggregation rate (d^{-1}); w_s: sinking velocity of dust particles $(m\ d^{-1})$; "-": process not included in the model; and "Name" shows runs used in the comparison (Figure A1).

Yücel et al., 2011). Considering these sources of iron in the model could on the one hand require a stronger scavenging, but on the other hand, with the colloidal pumping as an additional removal pathway of dissolved iron, one would need a smaller scavenging rate of free iron to reproduce observed dissolved iron distribution. For a holistic understanding of the role of lithogenic particles in the global iron cycle, more processes delivering lithogenic particles and iron should be included in models, for example, sediment resuspension and hydrothermal input.

Appendix A

A1. Sensitivity Runs With Respect To Processes Affecting the Particle Cycle

In total, 40 sensitivity runs have been performed with respect to processes affecting the particle cycle (Tables A1 and A2). A qualitative comparison of some selected runs is presented in section A2.

A2. Selected Sensitivity Runs With Respect To Particle Aggregation and Disaggregation

Five selected sensitivity runs are compared to illustrate the effect of different processes on the particle distribution qualitatively (Tables A1 and A2).

Considering the aggregation between dust and large particles only and ignoring disaggregation ("1 × aggr"), the concentration of particulate iron (pFe) decreases with depth throughout the water column (Figure A1). The decrease is stronger at the surface due to the aggregation with biogenic particles.

By considering the same aggregation and disaggregation additionally ("1 × aggr + disaggr"), the surface pFe becomes much higher because a part of the small dust particles is released from fast-sinking large aggregates. pFe increases considerably below its subsurface minimum (down to 1,000 m), as the concentration of biogenic particles decreases with depth rapidly and the loss of lithogenic particles through aggregation is thus diminished. In the deep ocean, disaggregation dominates the cycle of lithogenic particles.

If considering an additional aggregation among the small dust particles ("2 × aggr + disaggr"), pFe is significantly reduced at the surface where the aggregation among dust particles is at highest. A subsurface minimum is found at a similar depth as in 1 × aggr + disaggr. Below that, pFe increases again and reaches a

Table A2
Parameter Values Changed in Sensitivity Runs (B, Continued)

Run	k_{c2}	k_{c1}	k_{diss}	w_s	Name
17	1.6E−1	-	1.0E−2	0.2	
18	1.6E−1	-	2.0E−2	0.2	
19	1.6E−1	-	5.0E−2	0.2	
20	1.6E−1	-	1.0E−1	0.2	
21	1.6E−1	-	2.0E−1	0.2	
22	1.6E−1	-	5.0E−1	0.2	
23	1.6E−1	-	1.0	0.2	
24	1.6E−1	-	2.0	0.2	1 × aggr + disaggr
25	1.0E−1	-	1.0	0.2	
26	0.5E−1	-	1.0	0.2	
27	2.0E−1	-	1.0	0.2	
28	3.0E−1	-	1.0	0.2	
29	3.0E−1	-	1.0	0.2	
30	3.0E−1	-	1.0	0.2	
31	3.0E−1	-	5.0	0.2	
32	7.8E−2	2.6E−2	1.0	0.2	
33	3.1E−2	1.0E−2	1.0	0.2	
34	1.6E−2	5.2E−3	1.0	0.2	
35	7.8E−2	2.6E−2	1.5	0.2	
36	7.8E−2	2.6E−2	2.0	0.2	2 × aggr + disaggr
37	7.8E−2	2.6E−2	2.5	0.2	2 × aggr + higher disaggr
38	1.6E−1	5.2E−2	2.5	0.2	2 × higher aggr + higher disaggr
39	1.6E−1	5.2E−2	3.0	0.2	
40	3.1E−1	1.0E−1	3.0	0.2	

Note. k_{c2}: aggregation rate between dust and large particles ((mg/m^3)$^{-1}$ d^{-1}); k_{c1}: aggregation rate of dust particles ((mg/m^3)$^{-1}$ d^{-1}); k_{diss}: disaggregation rate (d^{-1}); w_s: sinking velocity of dust particles (m d^{-1}); -: process not included in the model; and Name shows runs used in the comparison (Figure A1).

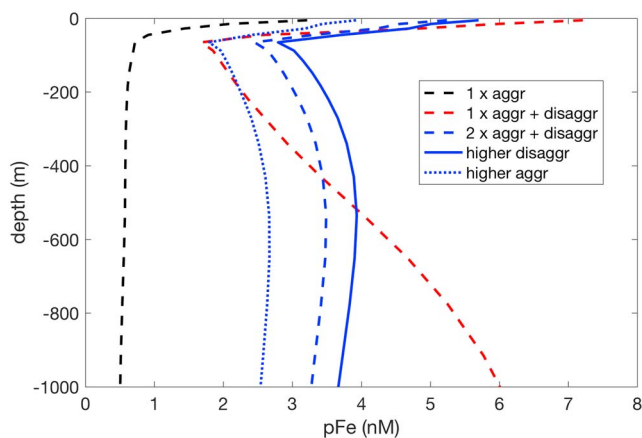**Figure A1.** Iron contained in all lithogenic particles (μmol Fe m^{-3}) in the model at ∼10°N along the CLIVAR A16N section.
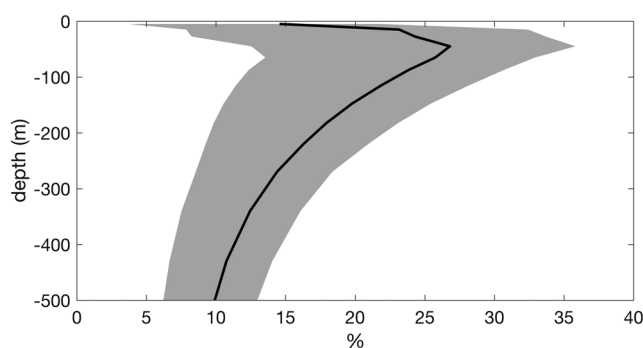
Figure A2. Modeled ratio of the coarse to total lithogenic particles (%) near Cape Verde. Black line: annual mean and gray area: seasonal variations.

deep maximum between 400 and 500 m. In the deep ocean, pFe just slightly decreases with depth, which is controlled by the balance between aggregation and disaggregation of lithogenic particles.

Using a higher disaggregation rate ("2 × aggr + higher disaggr") and both a higher aggregation and a higher disaggregation rate ("2 × higher aggr + higher disaggr"), we can change the absolute concentrations of pFe and just to some degree the form of its profile, for example, increasing the disaggregation rate leads to the formation of a clearer subsurface minimum. However, in all the sensitivity runs including two aggregation processes and disaggregation, the surface maximum of pFe is higher than its deep maximum. The possible explanations are presented in section 3.1.

The run presented in the manuscript as +Lith is equal to 2 × aggr + higher disaggr.

A3. Coarse Fraction of Lithogenic Particles

Ohnemus and Lam (2015) showed that about 10–60% of pFe in the upper 500 m near Cape Verde consists of coarse lithogenic particles. In the +Lith run, the coarse fraction at the same location is 5–35% with significant seasonal variations (Figure A2). The highest fractions are found in spring, when both the dust deposition flux from Mahowald et al. (2005) and the abundance of biogenic particles are high. In vertical, a subsurface maximum of the coarse fraction between 50 and 100 m is consistent with the pattern in Ohnemus and Lam (2015). Our modeled coarse fraction is, however, lower than the observed one, which could be probably explained by the difference between the strength of particle aggregation after individual dust events and that driven by monthly averaged deposition (see section 3.1).

References

Anderson, R. F., Cheng, H., Edwards, R. L., Fleisher, M. Q., Hayes, C. T., Huang, K.-F., . . . Shelley, R. U. (2016). How well can we quantify dust deposition to the ocean? *Philosophical Transactions of the Royal Society of London A: Mathematical, Physical and Engineering Sciences*, *374*, 2081. https://doi.org/10.1098/rsta.2015.0285

Antonov, J. I., Seidov, D., Boyer, T. P., Locarnini, R. A., Mishonov, A. V., Garcia, H. E., . . . Johnson, D. R. (2010). In S. Levitus (Ed.), *World Ocean Atlas 2009, Volume 2: Salinity* (pp. 184). Washington, DC: NOAA Atlas NESDIS 69, U.S. Government Printing Office.

Aumont, O., Ethé, C., Tagliabue, A., Bopp, L., & Gehlen, M. (2015). PISCES-v2 : An ocean biogeochemical model for carbon and ecosystem studies. *Geoscientific Model Development*, *8*(8), 2465–2513. https://doi.org/10.5194/gmd-8-2465-2015

Baker, A. R., & Croot, P. L. (2010). Atmospheric and marine controls on aerosol iron solubility in seawater. *Marine Chemistry*, *120*(1), 4–13. https://doi.org/10.1016/j.marchem.2008.09.003

Barkmann, W., Schäfer-Neth, C., & Balzer, W. (2010). Modelling aggregate formation and sedimentation of organic and mineral particles. *Journal of Marine Systems*, *82*(3), 81–95. https://doi.org/10.1016/j.jmarsys.2010.02.009

Barrett, P. M., Resing, J. A., Buck, N. J., Buck, C. S., Landing, W. M., & Measures, C. I. (2012). The trace element composition of suspended particulate matter in the upper 1000 m of the eastern North Atlantic Ocean: A16N. *Marine Chemistry*, *142–144*, 41–53. https://doi.org/10.1016/j.marchem.2012.07.006

Barrett, P. M., Resing, J. A., Buck, N. J., Landing, W. M., Morton, P. L., & Shelley, R. U. (2015). Changes in the distribution of al and particulate fe along A16N in the eastern North Atlantic ocean between 2003 and 2013: Implications for changes in dust deposition. *Marine Chemistry*, *177*, 57–68. https://doi.org/10.1016/j.marchem.2015.02.009

Bergquist, B. A., & Boyle, E. A. (2006). Dissolved iron in the tropical and subtropical Atlantic Ocean. *Global Biogeochemical Cycles*, *20*, GB1015. https://doi.org/10.1029/2005GB002505

Bishop, J. K. B., Davis, R. E., & Sherman, J. T. (2002). Robotic observations of dust storm enhancement of carbon biomass in the North Pacific. *Science*, *298*(5594), 817–21. https://doi.org/10.1126/science.1074961

Bonnet, S., & Guieu, C. (2004). Dissolution of atmospheric iron in seawater. *Geophysical Research Letters*, *31*, L03303. https://doi.org/10.1029/2003GL018423

Burd, A. B. (2013). Modeling particle aggregation using size class and size spectrum approaches. *Journal of Geophysical Research: Oceans*, *118*, 3431–3443. https://doi.org/10.1002/jgrc.20255

Campin, J.-M., & Goosse, H. (1999). Parameterization of density-driven downsloping flow for a coarse-resolution ocean model in *z*-coordinate. *Tellus A*, *51*, 412–430. https://doi.org/10.1034/j.1600-0870.1999.t01-3-00006.x

Clegg, S. L., & Whitfield, M. (1991). A generalized model for the scavenging of trace metals in the open ocean—II. Thorium scavenging. *Deep Sea Research Part A, Oceanographic Research Papers*, *38*(1), 91–120. https://doi.org/10.1016/0198-0149(91)90056-L

Clegg, S. L., Bacon, M. P., & Whitfield, M. (1991). Application of a generalized scavenging model to thorium isotope and particle data at equatorial and high-latitude sites in the Pacific Ocean. *Journal of Geophysical Research*, *96*(C11), 20,655–20,670.

Cochran, J. K., Buesseler, K. O., Bacon, M. P., & Livingston, H. D. (1993). Thorium isotopes as indicators of particle dynamics in the upper ocean: results from the JGOFS North Atlantic Bloom experiment. *Deep-Sea Research Part I*, *40*(8), 1569–1595. https://doi.org/10.1016/0967-0637(93)90017-W

Conway, T. M., & John, S. G. (2014). Quantification of dissolved iron sources to the North Atlantic Ocean. *Nature*, *511*, 212–215. https://doi.org/10.1038/nature13482

Croot, P. L., Streu, P., & Baker, A. R. (2004). Short residence time for iron in surface seawater impacted by atmospheric dry deposition from Saharan dust events. *Geophysical Research Letters*, *31*, L23S08. https://doi.org/10.1029/2004GL020153

Duce, R. A., & Tindale, N. W. (1991). Atmospheric transport of iron and its deposition in the ocean. *Limnology and Oceanography*, *36*(8), 1715–1726.

Elrod, V. A. (2004). The flux of iron from continental shelf sediments: A missing source for global budgets. *Geophysical Research Letters*, *31*(12), 2–5. https://doi.org/10.1029/2004GL020216

Geider, R. J., & La Roche, J. (1994). The role of iron in phytoplankton photosynthesis and the potential for iron-limitation of primary productivity in the sea. *Photosynthesis Research*, *39*, 275–301.

Geider, R. J., Macintyre, H. L., & Kana, T. M. (1998). A dynamic regulatory model of phytoplanktonic acclimation to light, nutrients, and temperature. *Limnology and oceanography*, *43*(4), 679–694.

Gent, P. R., & McWilliams, J. C. (1990). Isopycnal mixing in ocean circulation models. *Journal of Physical Oceanography*, *20*(1), 150–155. https://doi.org/10.1175/1520-0485(1990)020<0150:IMIOCM>2.0.CO;2

Guieu, C., Aumont, O., Paytan, A., Bopp, L., Law, C. S., Mahowald, N. . . . Völker, C. (2014). The significance of the episodic nature of atmospheric deposition to low nutrient low chlorophyll regions. *Global Biogeochemical Cycles*, *28*, 1179–1198. https://doi.org/10.1002/2014GB004852

Hauck, J., & Völker, C. (2015). Rising atmospheric CO_2 leads to large impact of biology on Southern Ocean CO_2 uptake via changes of the Revelle factor. *Geophysical Research Letters*, *41*, 1–7. https://doi.org/10.1002/2015GL063070.1

Hauck, J., Völker, C., Wang, T., Hoppema, M., Losch, M., & Wolf-Gladrow, D. A. (2013). Seasonally different carbon flux changes in the Southern Ocean in response to the Southern Annular Mode. *Global Biogeochemical Cycles*, *27*, 1236–1245. https://doi.org/10.1002/2013GB004600

Honeyman, B. D., & Santschi, P. H. (1989). A Brownian-pumping model for oceanic trace metal scavenging: Evidence from Th isotopes. *Journal of Marine Research*, *47*(4), 951–992. https://doi.org/10.1357/002224089785076091

Jackson, G. A., & Burd, A. B. (1998). Aggregation in the marine environment. *Environmental Science & Technology*, *32*(19), 2805–2814.

Jickells, T. D. (1999). The input of dust-derived elements to the Sargasso Sea: A synthesis. *Marine Chemistry*, *68*, 5–14.

Jickells, T. D., An, Z. S., Andersen, K. K., Baker, A. R., Bergametti, G., Brooks, N., . . . Torres, R. (2005). Global iron connections between desert dust, ocean biogeochemistry, and climate. *Science*, *308*(5718), 67–71. https://doi.org/10.1126/science.1105959

Key, R. M., Kozyr, A., Sabine, C. L., Lee, K., Wanninkhof, R., Bullister, J. L., . . . Peng, T.-H. (2004). A global ocean carbon climatology: Results from Global Data Analysis Project (GLODAP). *Global Biogeochemical Cycles*, *18*, GB4031. https://doi.org/10.1029/2004GB002247

Kriest, I., & Oschlies, A. (2008). On the treatment of particulate organic matter sinking in large-scale models of marine biogeochemical cycles. *Biogeosciences*, *5*(1), 55–72. https://doi.org/10.5194/bgd-4-3005-2007

Lam, P. J., Ohnemus, D. C., & Auro, M. E. (2015). Size-fractionated major particle composition and concentrations from the US GEOTRACES North Atlantic Zonal Transect. *Deep Sea Research Part II: Topical Studies in Oceanography*, *116*, 303–320. https://doi.org/10.1016/j.dsr2.2014.11.020

Lambert, F., Delmonte, B., Petit, J. R., Bigler, M., Kaufmann, P. R., Hutterli, M. A., . . . Maggi, V. (2008). Dust-climate couplings over the past 800,000 years from the EPICA Dome C ice core. *Nature*, *452*, 616–619. https://doi.org/10.1038/nature06763

Large, W. G., & Yeager, S. (2008). The global climatology of an interannually varying air–sea flux data set. *Climate Dynamics*, *33*, 341–364. https://doi.org/10.1007/s00382-008-0441-3

Liu, X., & Millero, F. J. (2002). The solubility of iron in seawater. *Marine Chemistry*, *77*(1), 43–54. https://doi.org/10.1016/S0304-4203(01)00074-3

Locarnini, R. A., Mishonov, A. V., Antonov, J. I., Boyer, T. P., Garcia, H. E., Baranova, O. K., . . . Johnson, D. R. (2010). In S. Levitus (Ed.), *World Ocean Atlas 2009, Volume 1: Temperature*. Washington, DC: NOAA Atlas NESDIS 68, U.S. Government Printing Office.

Losch, M., Menemenlis, D., Campin, J.-M., Heimbach, P., & Hill, C. (2010). On the formulation of sea-ice models. Part 1: Effects of different solver implementations and parameterizations. *Ocean Modelling*, *33*(1-2), 129–144. https://doi.org/10.1016/j.ocemod.2009.12.008

Mahowald, N., Kohfeld, K., Hansson, M., Balkanski, Y., Harrison, S., Prentice, I., . . . Rodhe, H. (1999). Dust sources and deposition during the last glacial maximum and current climate: A comparison of model results with paleodata from ice cores and marine sediments. *Journal of Geophysical Research*, *104*, 15,895–15,916.

Mahowald, N. M., Baker, A. R., Bergametti, G., Brooks, N., Duce, R. A., Jickells, T. D., . . . Tegen, I. (2005). Atmospheric global dust cycle and iron inputs to the ocean. *Global Biogeochem. Cycles*, *19*, GB4025. https://doi.org/10.1029/2004GB002402

Marshall, J., Adcroft, A., Hill, C., Perelman, L., & Heisey, C. (1997). A finite-volume, incompressible Navier Stokes model for studies of the ocean on parallel computers. *Journal of Geophysical Research*, *102*(C3), 5753–5766. https://doi.org/10.1029/96JC02775

Martin, J. (1990). Glacial-interglacial CO_2 change: The iron hypothesis. *Paleoceanography*, *5*, 1–13.

Measures, C. I., Landing, W. M., Brown, M. T., & Buck, C. S. (2008). High-resolution Al and Fe data from the Atlantic Ocean CLIVAR-CO_2 Repeat Hydrography A16N transect: Extensive linkages between atmospheric dust and upper ocean geochemistry. *Global Biogeochemical Cycles*, *22*, GB1005. https://doi.org/10.1029/2007GB003042

Murnane, R. J. (1994). Determination of thorium and particulate matter cycling parameters at station P: A reanalysis and comparison of least squares techniques. *Journal of Geophysical Research*, *99*(C2), 3393–3405. https://doi.org/10.1029/93JC03155

Murnane, R. J., Cochran, J. K., & Sarmiento, J. L. (1994). Estimates of particle- and thorium-cycling rates in the northwest Atlantic Ocean. *Journal of Geophysical Research*, *99*(C2), 3373–3392. https://doi.org/10.1029/93JC02378

Murnane, R. J., Cochran, J. K., Buesseler, K. O., & Bacon, M. P. (1996). Least-squares estimates of thorium, particle, and nutrient cycling rate constants from the JGOFS North Atlantic Bloom Experiment. *Deep-Sea Research Part I: Oceanographic Research Papers*, *43*(2), 239–258. https://doi.org/10.1016/0967-0637(96)00004-0

Nozaki, Y., Yang, H., & Yamada, M. (1987). Scavenging of thorium in the ocean. *Journal of Geophysical Research*, *92*(C1), 772–778. https://doi.org/10.1029/JC092iC01p00772

Ohnemus, D. C., & Lam, P. J. (2015). Cycling of lithogenic marine particles in the US GEOTRACES North Atlantic transect. *Deep Sea Research Part II: Topical Studies in Oceanography*, *116*, 283–302. https://doi.org/10.1016/j.dsr2.2014.11.019

Petit, J. R., Jouzel, J., Raynaud, D., Barkov, N. I., Barnola, J.-M., Basile, I., . . . Stievenard, M. (1999). Climate and atmospheric history of the past 420,000 years from the Vostok ice core, Antarctica. *Nature*, *399*, 429–436. https://doi.org/10.1038/20859

Pohl, C., Croot, P. L., Hennings, U., Daberkow, T., Budeus, G., & Loeff, M. R. V. (2011). Synoptic transects on the distribution of trace elements (Hg, Pb, Cd, Cu, Ni, Zn, Co, Mn, Fe, and Al) in surface waters of the Northern- and Southern East Atlantic. *Journal of Marine Systems*, *84*(1-2), 28–41. https://doi.org/10.1016/j.jmarsys.2010.08.003

Resing, J. A., Sedwick, P. N., German, C. R., Jenkins, W. J., Moffett, J. W., Sohst, B. M., & Tagliabue, A. (2015). Basin-scale transport of hydrothermal dissolved metals across the South Pacific Ocean. *Nature*, *523*, 200–206.

Revels, B. N., Ohnemus, D. C., Lam, P. J., Conway, T. M., & John, S. G. (2015). The isotopic signature and distribution of particulate iron in the North Atlantic Ocean. *Deep Sea Research Part II: Topical Studies in Oceanography*, *116*, 321–331. https://doi.org/10.1016/j.dsr2.2014.12.004

Rose, A. L., & Waite, T. D. (2007). Reconciling kinetic and equilibrium observations of iron(III) solubility in aqueous solutions with a polymer-based model. *Geochimica et Cosmochimica Acta*, *71*(23), 5605–5619. https://doi.org/10.1016/j.gca.2007.02.024

Sarthou, G., Baker, A. R., Kramer, J., Laan, P., Laës, A., Ussher, S. J., . . . Blain, S. (2007). Influence of atmospheric inputs on the iron distribution in the subtropical North-East Atlantic Ocean. *Marine Chemistry*, *104*(3-4), 186–202. https://doi.org/10.1016/j.marchem.2006.11.004

Schartau, M., Engel, A., Schröter, J., Thoms, S., Völker, C., & Wolf-Gladrow, D. (2007). Modelling carbon overconsumption and the formation of extracellular particulate organic carbon. *Biogeosciences Discussions*, *4*(1), 13–67. https://doi.org/10.5194/bgd-4-13-2007

Tagliabue, A., Bopp, L., Dutay, J.-C., Bowie, A. R., Chever, F., Jean-Baptiste, P., . . . Jeandel, C. (2010). Hydrothermal contribution to the oceanic dissolved iron inventory. *Nature Geoscience*, *3*(4), 252–256. https://doi.org/10.1038/ngeo818

Tagliabue, A., Mtshali, T., Aumont, O., Bowie, A. R., Klunder, M. B., Roychoudhury, A., & Swart, S. (2012). A global compilation of dissolved iron measurements: Focus on distributions and processes in the Southern Ocean. *Biogeosciences*, *9*(1), 1–17. https://doi.org/10.5194/bg-9-1-2012

Tagliabue, A., Aumont, O., DeAth, R., Dunne, J. P., Dutkiewicz, S., Galbraith, E., . . . Yool, A. (2015). How well do global ocean biogeochemistry models simulate dissolved iron distributions? *Global Biogeochemical Cycles*, *30*, 149–174. https://doi.org/10.1002/2015GB005289

Ussher, S. J., Achterberg, E. P., Powell, C., Baker, A. R., Jickells, T. D., Torres, R., & Worsfold, P. J. (2013). Impact of atmospheric deposition on the contrasting iron biogeochemistry of the North and South Atlantic Ocean. *Global Biogeochemical Cycles*, *27*, 1096–1107. https://doi.org/10.1002/gbc.20056

Völker, C., & Tagliabue, A. (2015). Modeling organic iron-binding ligands in a three-dimensional biogeochemical ocean model. *Marine Chemistry*, *173*, 67–77. https://doi.org/10.1016/j.marchem.2014.11.008

Wadley, M. R., Jickells, T. D., & Heywood, K. J. (2014). The role of iron sources and transport for Southern Ocean productivity. *Deep Sea Research Part I*, *87*, 82–94. https://doi.org/10.1016/j.dsr.2014.02.003

Wagener, T., Guieu, C., & Leblond, N. (2010). Effects of dust deposition on iron cycle in the surface Mediterranean Sea: Results from a mesocosm seeding experiment. *Biogeosciences*, *7*(11), 3769–3781. https://doi.org/10.5194/bg-7-3769-2010

Ye, Y., Wagener, T., Völker, C., Guieu, C., & Wolf-Gladrow, D. A. (2011). Dust deposition: Iron source or sink? A case study. *Biogeosciences*, *8*(8), 2107–2124. https://doi.org/10.5194/bg-8-2107-2011

Yücel, M., Gartman, A., Chan, C. S., & Luther, G. W. (2011). Hydrothermal vents as a kinetically stable source of iron-sulphide-bearing nanoparticles to the ocean. *Nature Geoscience*, *4*, 367–371. https://doi.org/10.1038/ngeo1148